The Analysis of High-Speed Railway Seismic-induced Track Geometric Irregularity

Guolong Li[1], Fei Yang[1], Mangmang Gao[1], Wentao Sun[2], and Xiangyu Qu[3,*]

[1] Infrastructure Inspection Research Institute, China Academy of Railway Sciences Corporation Limited, 100081 Beijing, China, liguolong@rails.cn; yf2009@rails.cn; gaomang@rails.cn

[2] Railway Science & Technology Research & Development Center, China Academy of Railway Sciences Corporation Limited, 100081 Beijing, China, sunwt@rails.cn

[3] Institute of Sound and Vibration Research, University of Southampton, SO17 1BJ, Southampton, UK, xq2n20@soton.ac.uk

Abstract: The high-speed railway in China passes through various seismic zones. As the track geometric irregularity is a critical aspect impacting train operation safety and train-induced vibration, it is meaningful to investigate the influence of earthquakes on the seismic-induced track geometric irregularity of high-speed railways. To determine the impact of earthquakes on track conditions, a complete study was conducted using various earthquake magnitude levels (3.0 to 7.0), varied limiting train speeds, and different track structural types (ballasted and ballastless track). The track quality index, long-wave irregularities, 10 m chord measurement, and vehicle vibration are analysed to suggest the change of track geometric irregularity and its influence after the earthquake. At the same time, the vehicle-track analysis model is used to calculate the difference in vehicle vibration under different seismic-induced track conditions. The vehicle acceleration, the rate of wheel load reduction, derailment coefficient indicators are investigated. These results imply that earthquakes have an impact on high-speed railways, causing track geometric irregularities to shift, which may contribute to increased vibration while trains are running. Compared to the ballasted track, whose normal speed is 250 km/h, the ballastless track, whose nominal speed is 350 km/h, was affected by the earthquake less. According to data, earthquakes have an influence on long waves greater than 1 m. While small and moderate earthquakes have a minor effect on railway safety, they do have an effect on train operating comfort because vehicle vibration is amplified as a result of the seismic-induced track geometric irregularity being worse.

Keywords: High-speed railway; track geometric irregularity; seismic-induced response; train vibration; track quality index

1 Introduction

In recent years, the development of high-speed railways (HSR) has made significant progress in some regions such as East Asia, Europe, and Africa. More HSRs are being built in hilly areas and coastal seismic fault belts with significant seismic intensity [1], such as in western China and Japan. Due to this situation, the probability of high-speed railways interfering with earthquakes has also grown significantly. In natural disasters that endanger railway safety, earthquakes are difficult to forecast. Destructive earthquakes not only inflict direct damage to railway infrastructure, but can produce a variety of secondary catastrophes and even result in accidents such as high-speed train derailment and overturning. Therefore, the effect of earthquakes on high-speed rail systems has garnered increased attention.

Destructive earthquakes not only inflict direct damage to railway infrastructure, but can produce a variety of secondary catastrophes and even result in accidents such as high-speed train derailment and overturning [2, 3]. Thus, there is considerable interest in the damage to the railway structure caused by earthquakes, and various studies are being undertaken in this field. Seismic-induced track damage and deformation may be classified into two types: failure of track structural stability, e.g., track irregularities [4, 5], and failure of track underlying structures such as embankments [6, 7] and bridges [8]. Because bridges are the critical components of railway systems, the seismic response of bridges has attracted considerable research, including different bridge types: long-span bridges, [9], steel truss girder bridges [10], cable-stayed bridges [11]. Also, some numerical [12, 13] and analytical [14, 15] train-track-bridge models are established to investigate the dynamic seismic-induced response of the track structure.

Although certain extremely severe earthquakes might cause damage to the railway structure, the majority of earthquakes are less severe. It can be found that the earthquake will not cause damage to the track's subgrade or bridge construction, but it will impair the track's stability, irregularity, and residual stress and deformation [16]. These irregularities grow may lead to extra train vibration. Track irregularity is one of the main factors for the vibration of railway vehicles. If the roughness of the track is severer after the earthquake, the train vibration and the wheel-rail force induced by the track irregularity will grow with the increase of the speed of the vehicle, which cannot be ignored. The earthquakes and track irregularities are often combined considered. Stochastic analysis model is built for investigating the dynamic track response [17]. The influence of train speed and seismic wave propagation velocity on the random vibration characteristics of the bridge and train are discussed by using the pseudo-excitation method [18]. However, the above studies mainly focused on the track irregularities influence when the earthquake occurred. Actually, the earthquake could induce more severer track irregularities. The seismic-induced geometric irregularity of rail

alignment is investigated. The amplitude for seismic-induced track irregularity significantly increases with the increase of earthquake intensity [19]. Additionally, the power spectral density curve of track geometry irregularity is considered and studied when transverse random earthquakes occur [20, 21]. The effects of track irregularity and seismic stresses on the dynamic response of the vehicle system demonstrated that track irregularity may greatly enhance the vehicle system's dynamic response [22]. Using both measured U.S. earthquake data and a finite element model, the frequency-domain distribution of earthquake-induced track irregularities was investigated [23]. However, the majority of these conclusions are based on model analysis and earthquake database library. Inadequate validation of track irregularities test data affected by the earthquake. The analysis of high-speed railway seismic-induced track geometric irregularity based on in-situ measurement data needs further explanation.

This paper measures and analyses the impact of track irregularities on several railway lines in China when subjected to seismic activity. Additionally, choose several typical irregularities from the measured data and do additional analysis using the vehicle-track coupling model. The impact of the track on the vibration of the vehicle is described when the track is affected by an earthquake and the track irregularity becomes severe. The in-situ measurement of track irregularities affected by the earthquake is introduced in Section 2. Then, the measurement data is statistically analysed in Section 3. Combined with a train-track model, the introduction of the model and calculation results are drawn in Section 4. The conclusion is shown in the end.

2 On-Site Measurement of Seismic-induced Geometric Irregularity

In reaction to the earthquakes that occurred in China during the last decade, special attention has been devoted to the railway infrastructure around the epicentre. Sense,t track irregularities impair driving safety and cause vibrations, it is essential to consider the effect of earthquakes on track conditions. The geometry of the track was compared before and after the earthquake. Track Quality Index (TQI) variation and the amplitude of track irregularities were determined twice before and following the earthquake. The measurement data is shown below, including the train's limited speed 250 km/h ballasted track and 350 km/h ballastless track that was severely damaged by the earthquake in all tested cases.

Numerous in-situ measurements were performed including the track irregularity of longitudinal level, alignment level, gauge, cross-level, and twist on the ballastless track designed for 350 km/h HSR, and ballasted track designed for 250 km/h HSR.

The situation of the site is shown in Figure 1 (a). The deformation and track irregularity under earthquake effects can be observed in the photographs of the site and detected by the track geometry car shown in Figure 1 (b).

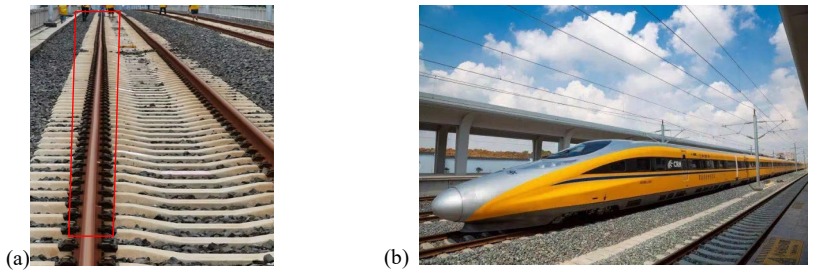

Figure 1
On-site measurement (a) Track geometry and (b) Track geometry car

The original data of the track longitudinal level, alignment, cross level and twist for ballastless track is shown in Figure 2. The red dashed box shows a distinct difference in the track geometric irregularity from the pre- and post-earthquake.

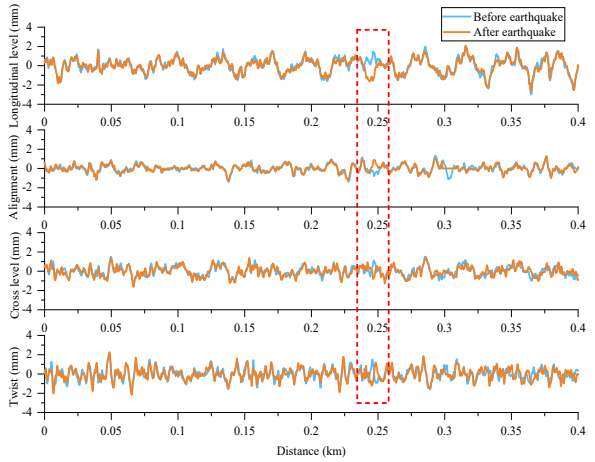

Figure 2
Original measurement data of track geometric irregularity.

The in-situ measurements data in Figure 2 indicated that the track geometric irregularity varies dramatically at the HSR beam junction locations. The earthquake caused the bridge piers to vibrate, which in turn caused the girders to vibrate and then lead to track deformation. Figure 3 illustrated the special sites where deformation is expected to occur marked in red dashed line.

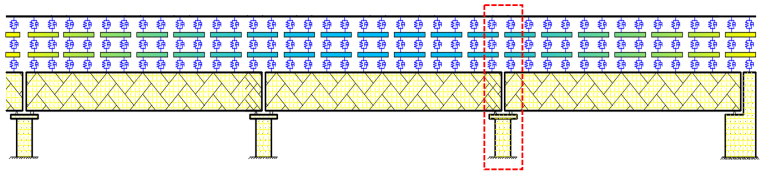

Figure 3
Beam junction locations

2.1 Track Geometric Irregularity

The waveform of long wave (1-120 m) and medium wave (1-42 m) can be analysed based on in-situ track irregularities data. The long wave affects the low frequency of the vehicle and vehicle ride comfort. Therefore, the long waveform of the track irregularity was selected for analysis. The details of the waveform of three cases are shown in Figure 4. As can be observed, the track irregularity has altered significantly in many areas with the effects of the earthquake.

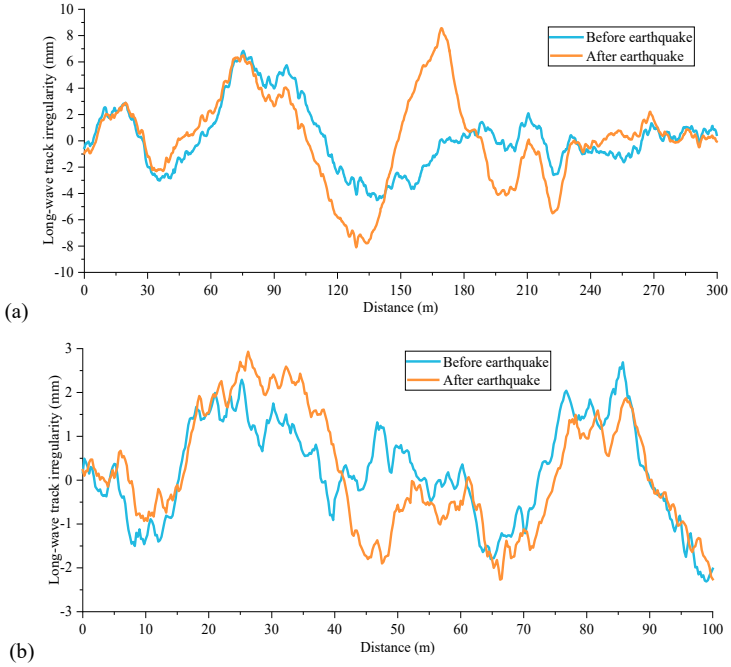

Figure 4
Long-waveform longitudinal level in (a) 250 km/h HSR track (b) 350 km/h HSR track

Long-wave track irregularity values up to 7 mm in certain locations of the 250 km/h HSR track owing to seismic events. The considerable change spans around 100 m. For the ballastless 350 km/h HSR track, the difference is also up to around 2 mm, the span of this area is nearly 40 m. These results demonstrate that the earthquake had a major effect on the rail structure's long-wave irregularity. The track's long-wave irregularity will affect the low-frequency train-induced vibration.

2.2 10 m-chord Measurement Method

The medium wave affected train safety. In this paper, the 10 m chord measurement method, a suitable method to describe the medium wave of track geometric irregularity, is used to measure the track irregularity data. The Chord measurement method [24] is a typical method to measure the track irregularities. Based on measurement data for pre-earthquake and post-earthquake, the left and right longitudinal level and alignment difference is shown in Figure 5.

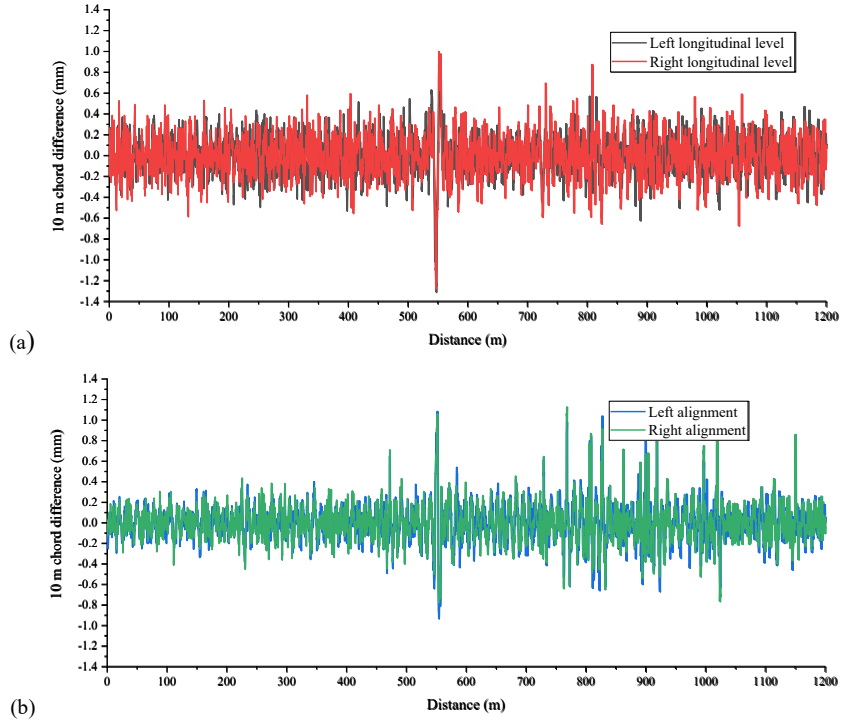

Figure 5
The difference of track irregularity based on 10m-chord method of 250 km/h HSR track including (a) longitudinal level and (b) alignment

According to the data in Figure 5. there is a significant disparity in longitudinal level and alignment. The longitudinal level has a maximum value of 1.4 mm. There is, however, no noticeable difference between the data for the left and right rails.

Figure 6 depicts the cumulative distribution of the difference between the output values of the 10 m-chord measurement before and after the earthquake at the ballasted track designed for 250 km/h HSR.

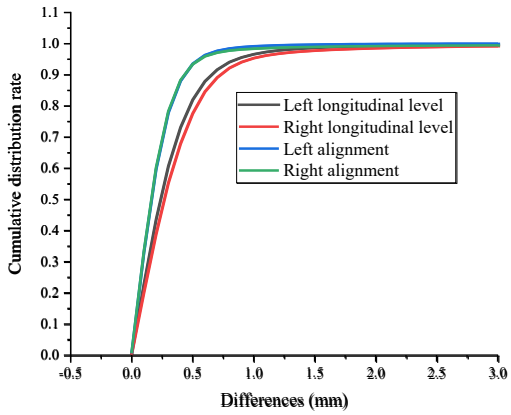

Figure 6
Cumulative distribution of the value difference of track irregularity

For 250 km/h high-speed railways, 95% of the cumulative distribution of the 10 m chordal measurements of track height before and after the earthquake is within 2 mm. Because the red and black lines, which indicate longitudinal level track irregularities, are lower than the blue and green lines, which show alignment track irregularities, particularly in the 0.5-1 mm difference range. As a result, the longitudinal level is more changeable than the track alignment, and the difference in track irregularities between the left and right rails is more noticeable.

2.3 Track Quality Index

Track Quality Index (TQI) [25] is a comprehensive index and assessment system that uses quantitative statistics to characterise the track's overall quality. It is the total of the standard deviations of the track irregularity in the vertical and horizontal direction, gauge, and twist irregularities elements. This number is directly connected to the overall track irregularity state, which shows the degree of dispersion of the track state in the 200 m segment. The larger the value, the more uneven and irregular the track is. It can be denoted as

$$\mathrm{TQI}=\sum_{i=1}^{7}\sqrt{\frac{1}{n}\sum_{j=1}^{n}\left(X_{ij}-\bar{X}_i^{\,2}\right)} \tag{1}$$

where X_{ij} means the magnitude of each geometric deviation in 200 m range of track. There are 7 standard deviations of items involved in evaluating track irregularities including the left longitudinal level, right longitudinal level, left alignment, right alignment, the track gauge, cross level and twist. n is the number of sampling points in 200 m range. $\bar{X}_i$ is the mean value of each project describing the track irregularities. It can be denoted as

$$\bar{X}_i=\frac{1}{n}\sum_{j=1}^{n}X_{ij} \tag{2}$$

In this part, three cases reflecting the track irregularity difference are chosen based on the measured track deformation degree data after the earthquake. The significant TQI changes measured data of 250 km/h and 350 km/h HSR track is chosen. A value is recorded every 200 metres, and the most visible gap of 10 kilometres is picked and shown in Figure 7.

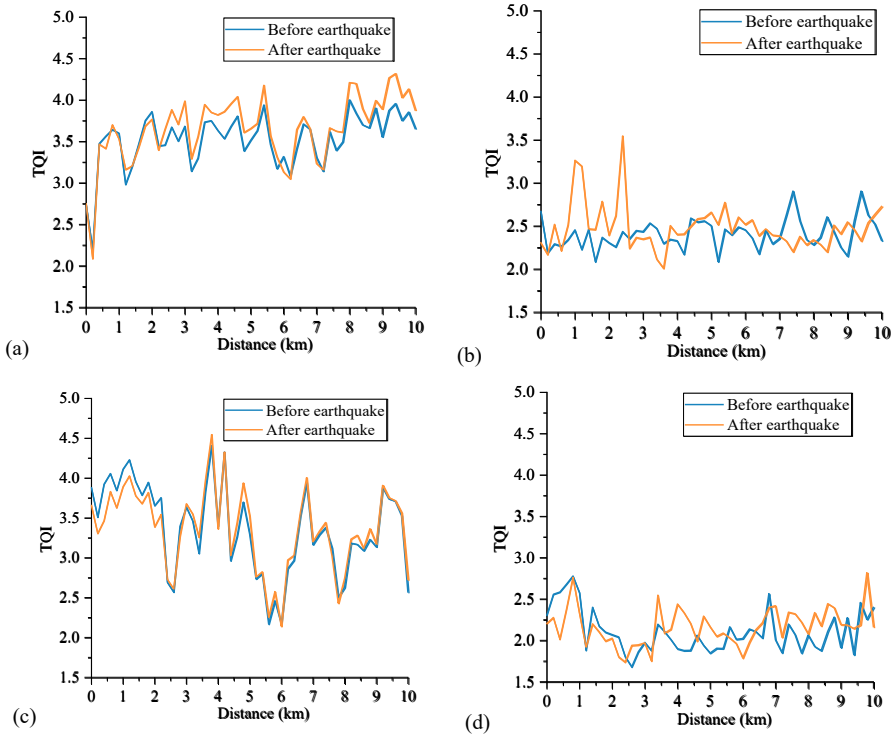

Figure 7

TQI difference influenced by the earthquake in (a) severe case from 350 km/h HSR ballastless track (b) severe case from 250 km/h HSR ballasted track (c) slight case from 350 km/h HSR ballastless track and (d) slight case from 250 km/h HSR ballasted track

It can be known that after the earthquake, although the TQI values have changed in selected regions, the difference is not statistically significant when observed in raw data. Sense, TQI is a comprehensive index for evaluating track conditions, it incorporates not only track height irregularity but also horizontal irregularity, gauge, and so forth. As a result, the general status of the track does not alter much after the earthquake.

The percentage of the seven components of the TQI evaluation indicators is shown in Figure 8. It includes the standard deviation for longitudinal level, alignment, track gauge, cross-level, and twist for ballasted and ballastless track that was severely and slightly impacted by the earthquake.

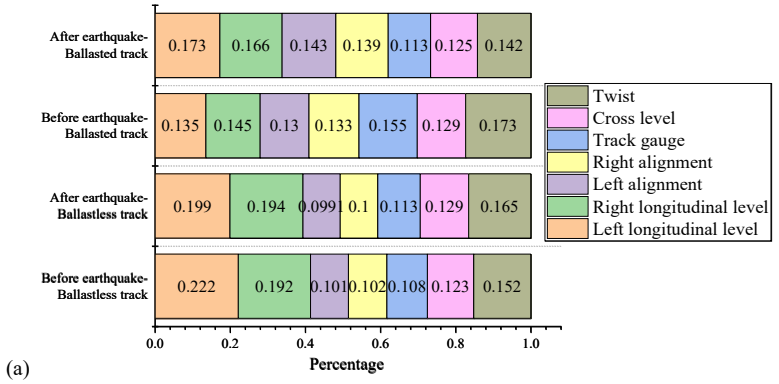

(a)

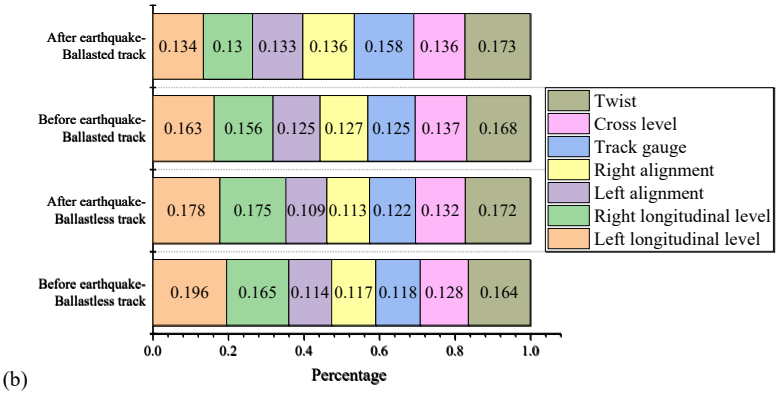

(b)

Figure 8

The percentage of 7 indicators from TQI evaluating the track influenced by the earthquake (a) severe case and (b) slight case

It can be seen that longitudinal level and twist account for a reasonably substantial amount of the overall TQI value when it comes to the contribution of each sub-factor to TQI values. Alignment track irregularities have a negligible impact on the TQI value. Less than track gauge and cross-level. The ballasted track exhibits

a comparatively high shift in longitudinal level and the gauge during seismic activity as compared to the ballastless track. In the case that the track is influenced by the earthquake significantly, due to seismic influences, the standard deviation of the longitudinal level is lower for the ballastless track, while the percentage rises for the ballasted track. Twist standard deviation demonstrates the inverse pattern. Therefore, the longitudinal level of track irregularities is the indicator most affected by the earthquake.

3 Analysis of Seismic-induced Geometric Irregularity of Track

Based on over 30 observations of the effect of earthquakes on track geometry during the last decade, the statistical results of TQI difference maximum value, long-waveform variations in the vertical direction, 10m-chord measurement value, and vehicle vertical acceleration are analysed. All statistical data of the earthquake is shown in Figure 9. This figure contains TQI difference maximum value, long-wave vertical differences, 95% cumulative value of 10 m-chard measurements and vehicle acceleration measured data of all the cases at 250 km/h HSR whose track form is mainly ballasted track (red) and 350 km/h HSR track whose track form is mainly ballastless track (blue). Different train speeds may cause different train-induced vibrations. The location of each bubble means the corresponding earthquake magnitude and peak ground acceleration (PGA, unit: cm/s^2) of each earthquake case. The size of each bubble means the evaluated value.

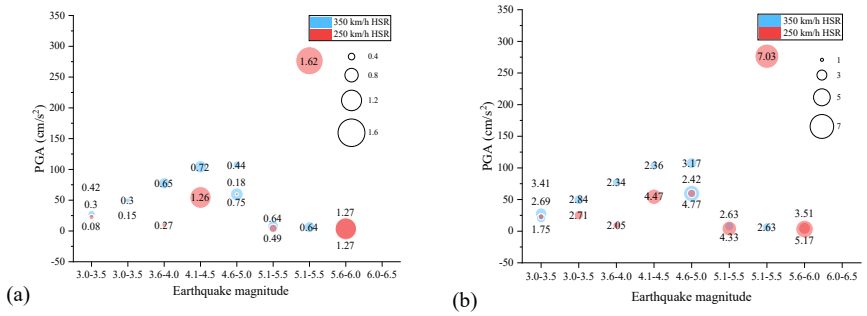

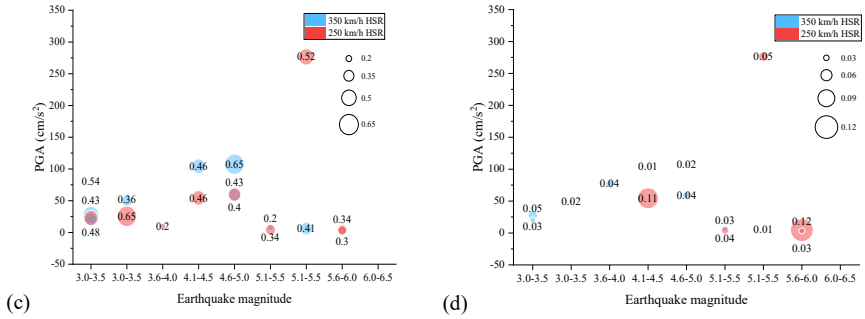

Figure 9

Statistical value of track irregularities (a)TQI difference max value (b) long wave vertical differences (unit: mm) (c) 95% cumulative value of 10 m chard measurement (unit: mm) (d) vehicle acceleration (unit: m/s^2).

The x axies is the earthquake magnitude scale, y axies is PGA values, which are critical for describing the effect and damage caused by earthquakes on infrastructure. In China, it can be determined by

$$PGA = C_0 + C_1 M + C_2 \lg R + C_3 T \tag{3}$$

where C_n is the factor, M represents earthquake magnitude, R means Epicentre distance. T is horizontal earthquake vector. More details can be found in [26].

Focus on the maximum difference value between TQI before the earthquake and after the earthquake, the value is located approximately in the range of 0-1.6. The value is greater for the ballasted track, indicating that the form of the ballasted track changes dramatically as a result of the earthquake. The long-wave irregularity and vehicle acceleration values follow the same rule, whose range is around 1-7 mm and 0-0.12 m/s^2 respectively. 95% cumulative value of 10 m chard measurement is in the range of 0.2-0.65 mm. It can be found that the larger the PGA value, the larger the 95% cumulative value of the 10 m chard measurement. According to data, TQI's different maximum values for 350 km/h tracks are less than 1, whereas some 250 km/h HSR tracks exceed 1. Similarly, the 350 km/h HSR track caused a change in vehicle vibration of less than 0.05 m/s^2 after the earthquake, but some of the 250 km/h HSR tracks induced a vehicle vibration change of more than 0.1 m/s^2 following the earthquake. Based on the monitoring and analysis of over 30 ballasted and ballastless tracks influenced by the seismic dynamics, it can be shown that earthquakes impair track geometric irregularities and further influence the safety and comfort of the train.

4 Vehicle-Track Analysis Model

4.1 Vehicle Model

The vehicle is modelled as a multibody system with 35 degrees of freedom (DOF). The vehicle is made up of one car body, two bogie frames, and four wheels. Each component has five DOFs, which include lateral movement, vertical movement, roll, pitch, and yaw. The sketch of the vehicle model is shown in Figure 10.

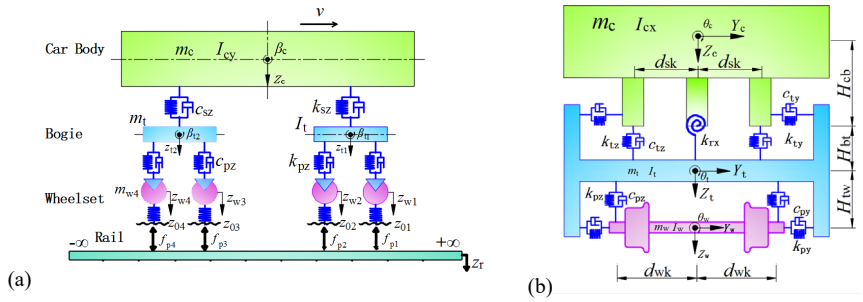

Figure 10

Vehicle dynamic analysis model (a) Side view of vehicle model(b) Front view of vehicle model

Kelvin springs, which are composed of a spring and a damping element, could be used to replicate the first and second suspensions, which can connect different multibody.

The model of the rail subsystem is constructed using two-layer nodes that correspond to the top and lower layers. The rail is a continuous Euler beam supported at discrete nodes by an elastic spring. The bottom node corresponds to the fastener position, and the spring-damper element between the upper and lower nodes corresponds to the elastic constraint imposed by the rubber pad under the rail.

4.2 Vehicle-Track Coupling Equation

The dynamic simulation analysis system is composed of the vehicle, track, which are connected by wheel-rail force. At all times, the system's vibration should adhere to force balance and deformation compatibility. The system's motion equation is as follows:

$$[M]\{\ddot{x}\}+[C]\{\dot{x}\}+[K]\{x\}=\{P\} \tag{4}$$

where $[M]$, $[C]$, and $[K]$ represent the mass, damping and stiffness matrix of the whole vehicle-track coupling model respectively. Thus, Eq. (4) can be written as

$$\begin{bmatrix} M_c & & \\ & M_r & \\ & & M_b \end{bmatrix}\begin{bmatrix} \ddot{x}_c \\ \ddot{x}_r \\ \ddot{x}_b \end{bmatrix}+\begin{bmatrix} C_{cc} & C_{cc} & \\ C_{rc} & C_{rr} & C_{rb} \\ & C_{br} & C_{bb} \end{bmatrix}\begin{bmatrix} \dot{x}_c \\ \dot{x}_r \\ \dot{x}_b \end{bmatrix}+\begin{bmatrix} K_{cc} & K_{cc} & \\ K_{rc} & K_{rr} & K_{rb} \\ & K_{br} & K_{bb} \end{bmatrix}\begin{bmatrix} x_c \\ x_r \\ x_b \end{bmatrix}=\begin{bmatrix} P_c \\ P_r \\ P_b \end{bmatrix} \tag{5}$$

The subscript *c* means car, *r* means rail, and *b* means ballast.

The details of the train and track parameters are shown in Ref. [27]. These values are expected to stabilise after the earthquake. The rail pad has a vertical static stiffness of 60 MN/m and a vertical damping of 75 kNs/m. The rail pad has a lateral static stiffness of 20 MN/m and a horizontal damping of 60 kNs/m.

The wheel-rail interaction force is simulated by Hertz nonlinear elastic contact theory. This theory can be adopted in the normal direction of wheel-rail contact. The vertical wheel-rail interaction force is denoted as

$$N_Z(t)=\left[\frac{1}{G}\delta Z(t)\right]^{3/2} \tag{6}$$

where G is the wheel-rail contact constant factor, whose unit is m/N$^{2/3}$. $\delta Z(t)$ is the elastic compression deformation between wheel and rail whose unit is m.

Kalker linear creep theory [28] is used to calculate the longitudinal, lateral, and rotational creep forces between wheel and rail.

$$\begin{cases} F_x=-f_{11}\xi_x \\ F_y=-f_{22}\xi_y-f_{23}\xi_\phi \\ M_z=f_{23}\xi_y-f_{33}\xi_\phi \end{cases} \tag{7}$$

where f_{ij} is the Kalker creep coefficient. ξ is creepage.

The Shen-Hedrick-Elkins theory [29] is utilised to perform nonlinear adjustments on the longitudinal and lateral creep slip forces between the wheel and rail.

The Newmark-β technique approach is used to solve the dynamic equations of the train, track, and under-track structure once they have been determined. Multiple iterations are required because the interaction between the subsystems at each time step is reliant on the system's response at that moment in time. The conditions of equilibrium of forces were used to calculate the interaction between the subsystems. As a consequence, the displacement difference between two successive iterations of the vehicle, rail, and under-rail structure at each time step meets the convergence condition's accuracy criterion. The highest precision in displacement is 0.1 μm.

4.3 Calculation Results

Four scenarios are selected to investigate the impact of seismic-induced track irregularity. It is said to include two types of tracks, ballastless track, and ballasted track, as well as two levels of earthquake-affected track irregularities. The term 'severely' refers to the fact that the track irregularities alter much after the earthquake. The term 'slightly' refers to the track irregularities not altered notably as a result of the earthquake. Four cases information is summarised in Table 1.

Table 1

Case summary

Case number	Track type	Track affected by earthquake
Case A	Ballastless track	Severely
Case B	Ballastless track	Slightly
Case C	Ballasted track	Severely
Case D	Ballasted track	Slightly

The power spectrum density of track longitudinal level is shown in Figure 11. From the PSD plot, it can be seen that the earthquakes have an influence on long waves from track irregularities greater than 10 m. For ballasted track, there is also a difference zone at wavenumber 0.1-0.3 (1/m) range which corresponding to the wavelength range 3-10 m.

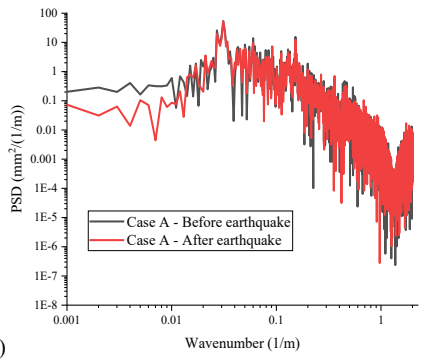

(a)

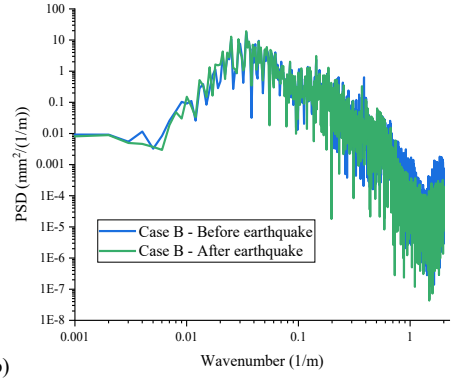

(b)

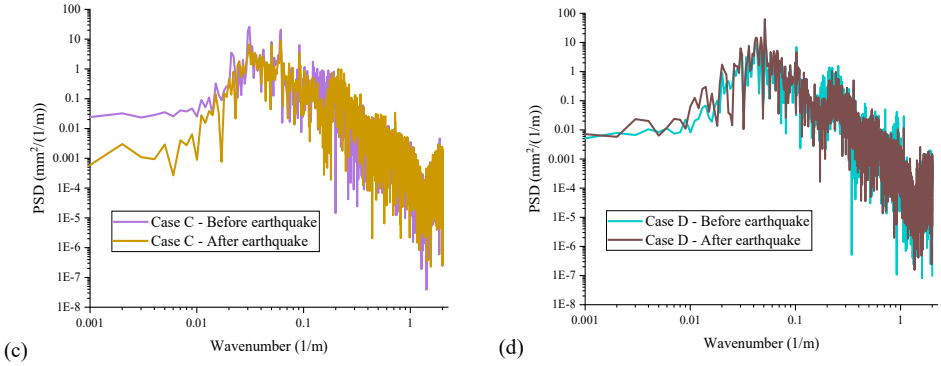

Figure 11

PSD of track irregularity longitudinal level from (a) Case A, (b) Case B, (c) Case C and (d) Case D.

The vehicle vibration, the rate of wheel load reduction, and derailment coefficient in time domain are shown in Figure 12. It can be known that within the green dashed line, the track geometric irregularity generated by the earthquake results in a more apparent deviation.

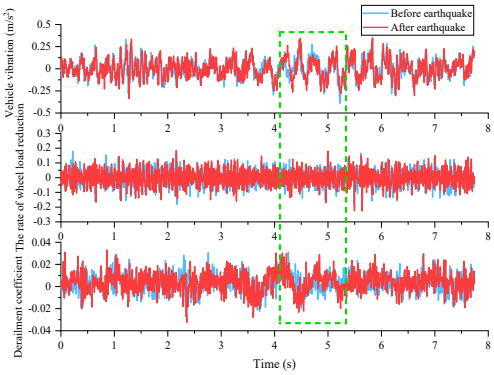

Figure 12

Vehicle vibration, the rate of wheel load reduction, and derailment coefficient in time domain.

4.3.1 Vehicle Acceleration

Focus on the vehicle acceleration, the maximum value and root mean square (RMS) value of acceleration in time domain is shown in Figure 13 corresponding to four cases introduced in Table 1.

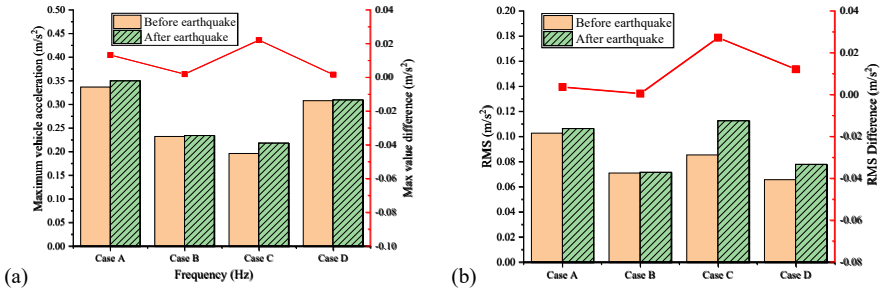

Figure 13

The vehicle acceleration value and differences (a) maximum value and (b) RMS value

The RMS value is calculated based on:

$$X_{\text{rms}} = \sqrt{\frac{\sum_{i=1}^{N} X_i^2}{N}} = \sqrt{\frac{X_1^2 + X_2^2 + \cdots + X_N^2}{N}} \tag{8}$$

where X_i means the data sample and N is the number of sampling point.

From Figure 13, it is shown that there is a considerable rise in the maximum value of vehicle vibration for conditions that are badly affected by the earthquake, and the difference in the maximum value of vehicle vibration for circumstances that are slightly impacted by the earthquake is not significant. Focus on the RMS value of vehicle acceleration increase based on seismic-induced track geometric irregularities increased, the ballasted track can lead to more vibration increase compared with the ballastless track.

All the results presented above assume that after the earthquake, the track irregularity is altered while the track parameters remain unchanged. In this section, the RMS values of the vehicle are investigated when the track's vertical parameters are modified after the earthquake. Case C after the earthquake is selected as the reference case, and the RMS values of the vehicle are summarized in Table 2.

Table 2

RMS value under different track parameters

Parameters: changed item	RMS value (m/s^2)
Vertical stiffness: 48 MN/m (increase 20%)	0.115
Vertical stiffness: 72 MN/m (decrease 20%)	0.111
Vertical damping: 60 kNs/m (increase 20%)	0.116
Vertical damping: 90 kNs/m (decrease 20%)	0.111

From the results, it is evident that reducing the vertical stiffness and damping of the track after the earthquake leads to an increased response of the train (Case C exhibits an RMS value of the vehicle as 0.1125 m/s^2).

4.3.2 The Rate of Wheel Load Reduction

The rate of wheel load reduction is an indicator to evaluate the train's safety. It can be calculated by:

$$P = \frac{\Delta P}{P_0} = \frac{P_2 - P_1}{P_2 + P_1} \tag{9}$$

where P is the rate of wheel load reduction ΔP is lowering load side wheels' heavy load reduction. P_0 is the average wheel weight. P_1 signifies the wheelset's decreasing wheel side, while P_2 denotes the wheelset's growing wheel side. The safety standard from Chinese standard is less than 0.65 for first limit related to vehicle operation security and less than 0.60 for second limit, which is related to safety allowance. The maximum value of the rate of wheel load reduction and the power spectrum density value of the rate of wheel load reduction before and after the seismic dynamic response is introduced in Figure 14.

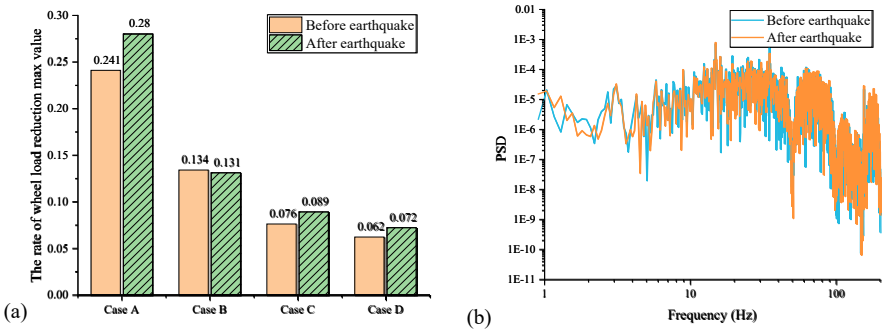

Figure 14

The rate of wheel load reduction (a) maximum value for one wheelset and (b) PSD value for case A

It can be known that for the ballastless track, the rate of wheel load reduction rises when the track is substantially affected by earthquakes and remains relatively constant when the track is not disturbed. When the ballasted track is also extensively affected by the earthquake, the rate of wheel load reduction rises, although not as much as on the ballastless track. Therefore, focusing on Case A, the PSD value is investigated. There is a significant difference in the 20-40 Hz frequency band. The rate of wheel load reduction above 50 Hz does not change significantly due to the track geometric irregularity caused by the earthquake.

4.3.3 Derailment Coefficient

The derailment coefficient is defined as the Q/P ratio of the lateral force Q to the vertical force P operating on the wheel at any given time. It can be denoted as

$$\frac{Q}{P} = \frac{\tan\alpha - \mu}{1 + \mu\tan\alpha} \tag{10}$$

where Q means the lateral force act on the wheel, P means the vertical force act on the wheel. μ means the fiction coefficient, α means the maximum flange contact angle. For rail safety considerations, the Chinese standard specifies that this indicator be smaller than 0.8.

The maximum value and Case A PSD value of derailment coefficient is shown in Figure 15.

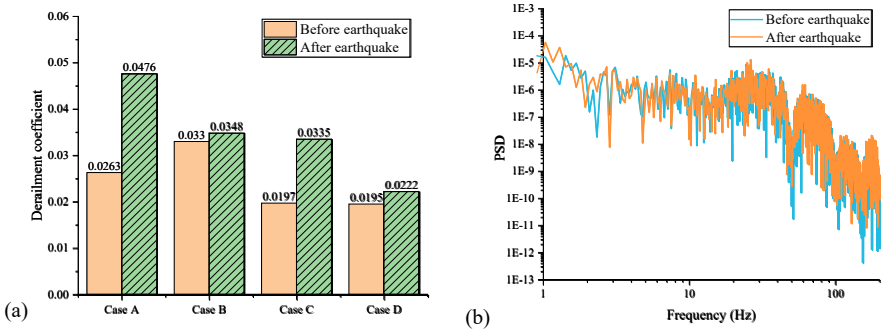

Figure 15

The derailment coefficient (a) maximum value and (b) PSD of Case A

From Figure 15, it can be seen that Case A has the highest derailment coefficient, followed by Case C. After the earthquake, the derailment coefficients for Cases B and D remain almost unchanged. The maximum value differences of derailment coefficient are from Case A, thus, the PSD value analysis from Case A is investigated. The main trend PSD of Case A is similar before and after the earthquake. There are some not very significant differences at 30 Hz and 150 Hz.

Although the derailment coefficient and rate of wheel load reduction have increased somewhat in maximum value as a result of the earthquake, they remain within the specification's normal range. This demonstrates that minor and moderate earthquakes have little effect on train operation safety.

Conclusion

The seismic-influenced track states of HSR were evaluated, as was the effect of earthquakes of various magnitudes level (3.0-7.0), different lines, and varied track types (ballasted and ballastless). Additionally, the impact of various earthquake-induced track irregularities on vehicle vibration are estimated and investigated

using the vehicle-track dynamic analysis model. Some conclusions can be summarised.

According to measurements and statistical analysis of the track state on-site after the earthquake in China, the earthquake had varying degrees of influence on the HSR track., The long-wave irregularity, 95% cumulative value of 10 m-chard measurements, and track quality index vehicle acceleration measured data are seen as the parameters for evaluating the seismic-induced track geometric irregularity. These parameters suggest that high-speed railways are affected by earthquakes which can produce a certain amount of track irregularities changes.

The statistical conclusions of TQI differences value, long-waveform vertical waveform, 10 m-chord measurement value, and vehicle vertical acceleration are analysed based on over 30 measurement sites of the influence of earthquakes on track geometry during the previous decade. For a ballast track with a nominal speed of 250 km/h, the TQI variation can reach a maximum of 1.6 and the track geometric irregularity variation of 1.4 mm obtained by 10 m chord measurement, both of which are greater than for a ballastless track with a nominal speed of 350 km/h, whose TQI variation value is up to 0.75, and track irregularity variation based on 10 m-chord method is around 1mm.

A train-track coupling model is built to calculate the train running safety and comfort under different track geometric irregularities. The ballasted track can induce higher train vibration. The maximum value from calculation results is around 0.45 m/s^2. The rate of wheel load reduction and derailment coefficient is higher for the ballastless track, whose value is up to 0.28 and 0.0476 respectively, compared with that indicator for the ballasted track. However, all of these indicators meet the requirement.

Acknowledgement

This research was funded by China State Railway Group Corporation Limited science foundation (No. P2021T013) and China Academy of Railway Sciences Corporation Limited science foundation (No.2021YJ250). The supports are gratefully acknowledged.

References

[1] A. Vijayakumar, H. Qian, The High-Speed Railway Bridges Under Vehicle Moving Load And Near Fault Seismic Ground Motions – Review, Journal of Building Materials and Structures, 8(2), 2021, pp. 115-127

[2] X. Xiao, L. Ling, X. Jin, A study of the derailment mechanism of a high speed train due to an earthquake, Vehicle System Dynamics, 50(3), 2012, pp. 449-470

[3] X. Wu, S. Liang, M. Chi, An investigation of rocking derailment of railway vehicles under the earthquake excitation, Engineering Failure Analysis, 117 2020

[4] Y. C. Cheng, C. T. Hsu, Derailment safety analysis for a tilting railway vehicle moving on irregular tracks shaken by an earthquake, Proceedings of the Institution of Mechanical Engineers, Part F: Journal of Rail and Rapid Transit, 230(3), 2014, pp. 625-642

[5] Z. Lai, X. Kang, L. Jiang, W. Zhou, Y. Feng, Y. Zhang, J. Yu, L. Nie, M. Bayat, Earthquake Influence on the Rail Irregularity on High-Speed Railway Bridge, Shock and Vibration, 2020 2020, pp. 1-16

[6] Y. Lin, G. Yang, Dynamic behavior of railway embankment slope subjected to seismic excitation, Natural Hazards, 69(1), 2013, pp. 219-235

[7] S. H. Ju, H. C. Li, Dynamic interaction analysis of trains moving on embankments during earthquakes, Journal of Sound and Vibration, 330(22), 2011, pp. 5322-5332

[8] X. Kang, L. Jiang, Y. Bai, C. C. Caprani, Seismic damage evaluation of high-speed railway bridge components under different intensities of earthquake excitations, Engineering Structures, 152 2017, pp. 116-128

[9] X. Gao, P. Duan, H. Qian, Dynamic response analysis of long-span continuous bridge considering the effect of train speeds and earthquakes, International Journal of Structural Stability and Dynamics, 20(06), 2020, 2040013

[10] Y. Feng, L. Jiang, W. Zhou, J. Han, Y. Zhang, L. Nie, Z. Tan, X. Liu, Experimental investigation on shear steel bars in CRTS II slab ballastless track under low-cyclic reciprocating load, Construction and Building Materials, 255 2020

[11] C. Yang, X. Cai, Seismic Response of a Cable-Stayed Bridge considering Non-uniform Excitation Effect: Model Design and Shake Table Testing, KSCE Journal of Civil Engineering, 26(1), 2021, pp. 286-297

[12] X. He, M. Kawatani, T. Hayashikawa, T. Matsumoto, Numerical analysis on seismic response of Shinkansen bridge-train interaction system under moderate earthquakes, Earthquake Engineering and Engineering Vibration, 10(1), 2011, pp. 85-97

[13] X. T. Du, Y. L. Xu, H. Xia, Dynamic interaction of bridge-train system under non-uniform seismic ground motion, Earthquake Engineering & Structural Dynamics, 41(1), 2012, pp. 139-157

[14] Y. B. Yang, Y. S. Wu, Dynamic stability of trains moving over bridges shaken by earthquakes, Journal of Sound and vibration, 258(1), 2002, pp. 65-94

[15] M. Tanabe, N. Matsumoto, H. Wakui, M. Sogabe, H. Okuda, Y. Tanabe, A simple and efficient numerical method for dynamic interaction analysis of a high-speed train and railway structure during an earthquake, Journal of Computational and Nonlinear Dynamics, 3(4), 2008

[16] L. Jiang, J. Yu, W. Zhou, W. Yan, Z. Lai, Y. Feng, Applicability analysis of high-speed railway system under the action of near-fault ground motion, Soil Dynamics and Earthquake Engineering, 139 2020

[17] L. Xu, W. Zhai, Stochastic analysis model for vehicle-track coupled systems subject to earthquakes and track random irregularities, Journal of Sound and Vibration, 407 2017, pp. 209-225

[18] Z. Zeng, Y. Zhao, W. Xu, Z. Yu, L. Chen, P. Lou, Random vibration analysis of train–bridge under track irregularities and traveling seismic waves using train–slab track–bridge interaction model, Journal of Sound and Vibration, 342 2015, pp. 22-43

[19] J. Yu, L. Jiang, W. Zhou, X. Liu, Z. Lai, Seismic-Induced Geometric Irregularity of Rail Alignment under Transverse Random Earthquake, Journal of Earthquake Engineering, 2022, pp. 1-22

[20] J. Yu, L. Jiang, W. Zhou, J. Lu, T. Zhong, K. Peng, Study on the influence of trains on the seismic response of high-speed railway structure under lateral uncertain earthquakes, Bulletin of Earthquake Engineering, 19(7), 2021, pp. 2971-2992

[21] J. Yu, L. Jiang, W. Zhou, X. Liu, Z. Lai, Evolutionary power spectrum density of earthquake-induced rail geometric irregularities, Structure and Infrastructure Engineering, 2022, pp. 1-16

[22] D. Mu, S. G. Gwon, D. H. Choi, Dynamic responses of a cable-stayed bridge under a high speed train with random track irregularities and a vertical seismic load, International Journal of Steel Structures, 16(4), 2016, pp. 1339-1354

[23] J. Yu, L. Jiang, W. Zhou, Study of the target earthquake-induced track irregularity spectrum under transverse random earthquakes, International Journal of Structural Stability and Dynamics, 22(16), 2022, 2250190

[24] L. Ma, H. Ouyang, C. Sun, R. Zhao, L. Wang, A curved 2.5D model for simulating dynamic responses of coupled track-tunnel-soil system in curved section due to moving loads, Journal of Sound and Vibration, 451 2019, pp. 1-31

[25] A. E. Fazio, J. Corbin, Track quality index for high speed track, Journal of transportation engineering, 112(1), 1986, pp. 46-61

[26] J. Zhuang, J. Peng, X. Zhu, W. Huang, Scenario-Based Risk Assessment of Earthquake Disaster Using Slope Displacement, PGA, and Population Density in the Guyuan Region, China, ISPRS International Journal of Geo-Information, 8(2), 2019

[27] S. Ma, L. Gao, X. Liu, J. Lin, Deep Learning for Track Quality Evaluation of High-Speed Railway Based on Vehicle-Body Vibration Prediction, IEEE Access, 7 2019, pp. 185099-185107

[28] J. J. Kalker, On the rolling contact of two elastic bodies in the presence of dry friction, Delft University, The Netherland, 1967

[29] Z. Shen, J. Hedrick, J. Elkins, A comparison of alternative creep force models for rail vehicle dynamic analysis, Vehicle System Dynamics, 12(1-3), 1983, pp. 79-83